Spallation of Copper Target Irradiated by a Relativistic High-Current Electron Beam: Experimental and Numerical Investigations[1]

A.B. Markov, S.A. Kitsanov, S.D. Korovin, I.K. Kurkan, S.D. Polevin, D.I. Proskurovsky, V.P. Rotshtein, A.P. Yalovets*, and A.E. Mayer*

Institute of High-Current Electronics, 2/3, Akademicheskii pr., Tomsk, 634055, Russia,
Phone: (3822) 491695, Fax: (3822) 492410, e-mail: almar@fromru.com
** Chelyabinsk State University, 129, Bratjev Kashirinykh st., Chelyabinsk, 454021, RussiaPresenting Author's*

Abstract – This paper presents the results of investigations of the rear surface spallation of copper targets irradiated with a relativistic high-current electron beam produced by the SINUS-7 accelerator. Special attempts were made to enhance the uniformity of the beam over its cross-section. The beam was formed in the cathode-grid-collector electrode system. The maximum electron energy, diode current, and pulse duration were 1.4 MeV, 25 kA, and 50 ns, respectively. The current density at the center of the beam, measured with a Faraday cup, was found to be about 8 kA/cm^2. The predicted results on the electron beam formation performed with the KARAT code is in good agreement with experimental data. A direct proportion between the spalled layer depth and the target thickness has been revealed in experimental investigations of the rear surface spallation. Scanning electron microscopy of the spalled surface has shown that the surface is cellular in structure with an average cell size of ~10 μm. This is evidence of the dynamic character of the spallation process. The temperature and stress fields in the target induced by the electron beam were simulated with the BETAIN1 numerical code based on solving hydrodynamic equations. Comparison of the predictions with experimental results has made it possible to determine the spall strength of copper. It has been found to be approximately 1.1 GPa at a strain rate of $5 \cdot 10^5$ s^{-1}. There is good agreement between the results obtained and the data available in the literature.

1. Introduction

The heat and strain processes induced in materials by pulsed power irradiation, particularly with intense pulsed electron beams, result in various types of modification of its structure and properties. Modification may take place both within and beyond the heat-affected zone (HAZ). However, in the HAZ the material is subject to heating and the action of stress fields, while beyond this zone there is almost no heating and the material is modified only due to the latter factor.

By now a large number of papers devoted to the modification of materials by nonrelativistic pulsed electron beams has been published [1, 2]. Usually, beams of pulse duration ~10^{-6}–10^{-5} s, which is much longer than the acoustic relaxation time, are used in industrial applications. The stress wave in this case has a low amplitude (less than 10^6 Pa) and does not cause undesirable modification of the material beyond the HAZ [3].

Investigations of the interaction of pulsed-power energy fluxes with matter resulting in the generation of a high-power stress wave, which, when reflected from the rear surface, causes spallation, are of great interest. In particular, investigations of the spall fracture at high strain rates are important in the physics of fast phenomena. The most commonly used investigation methods are the generation of stress waves by a plane-parallel plate impact and by explosion [4]. Besides, the method of stress wave generation by laser irradiation is now widely used [5–8]. The strain rate under laser irradiation can reach values more than 10^8 s^{-1}. The publications on the spallation induced by an electron beam are noticeably smaller in number notwithstanding certain advantages of electron beams. The much deeper depth of penetration of an electron beam into metallic materials compared to that of a laser beam enables spallation experiments both with thick specimens and with thin foils. In the latter case, the mode of heat impact is realized where the foil is uniformly and instantaneously heated beyond room temperature [9, 10]. The method of fracture investigations using the x-rays produced by a nuclear explosion is being developed [11].

It has been revealed [12] that the spall strength of a material, which is usually identified as the peak amplitude of the stress wave resulting in spallation, depends not only on the initial temperature of the target, but also on the loading conditions, in particular on the strain rate [12]. Sometimes the term “longevity“ is used as a loading characteristic, which is estimated as the time interval from the moment of energy delivery to the target to the moment of its fracture [9, 10, 13].

[1] This work was supported partially by Ministry of Education of RF and CRDF within the program BRHE (project No. 016-02).

The dependence of the fracture characteristics on the loading conditions means that the processes of nucleation, growth, and coalescence of microvoids or microcracks are sensitive to the intensity of the stresses and to the duration of their action. The above assumptions formed the basis for dynamic spallation models such as those developed by Tuler and Butcher [5] and Kanel [7]. Despite the long-term and advantageous research in this field, some problems remain unresolved. So far a universal spallation model has not been developed. Moreover, the spallation strength obtained for the same loading modes by different researchers varies sometimes appreciably [5, 7, 9].

The purpose of the present work was to investigate numerically the evolution of the stress waves and to estimate the strain rate and spall strength in a copper target irradiated with a relativistic high-current electron beam.

2. Electron Beam Equipment and Diagnostics

In these investigations, the relativistic high-current electron beam produced by the SINUS-7 accelerator [14] was used. The high-voltage generator of the accelerator is an oil-insulated coaxial pulse-forming line charged by a built-in Tesla transformer. A gas-filled spark gap is used as a high-voltage pulse switch. The pulse-forming line is matched to the vacuum diode through an oil-insulated transmission line.

The electron-beam was formed in a cathode-grid-collector electrode system, with the grid and collector being grounded. This system allows one to control the electron-beam parameters by selecting the cathode-grid and grid-collector gap. The optimum gap values were found to be l_1 = 15 mm and l_2 = 12–36 mm between the cathode and the grid and the grid and the collector, respectively. The cathode was a metal-dielectric plate measuring 30 mm in diameter. Two types of grids were used – one made of tungsten and the other made of steel with the transmission ratios being 0.7 and 0.85, respectively. The specimens to be irradiated were placed onto the collector. Figure 1 presents the calculated electron beam propagation for l_2 = 20 mm made with a KARAT numerical code [15]. It is evident that the electrons emitted from the cathode (*1*) reach the grid (*2*) and propagate further to the collector (*3*). Note that starting from a certain point in the drift space, the beam begins to compress under the self magnetic field. No beam pinching is, however, observed, and no virtual cathode is formed.

The diode voltage and current measurements were performed using a capacitive divider and a low-resistance shunt, respectively, which were built into the accelerator transmission line. In addition, the beam current was also taken by a low-resistance shunt in the collector circuit. The results are given in Fig. 2. It is evident that the maximum diode voltage, diode current, and beam current are 1.3 MV, 24 kA and 17 kA, respectively. The electron beam pulse duration is 50 ns. We have estimated from the waveforms that the fraction of the energy incident on the collector is approximately 70% of that stored in the pulse. The experimentally measured beam currents are in a satisfactory agreement with those estimated by the KARAT code, where for the same spacing values the maximum beam current was 13 kA.

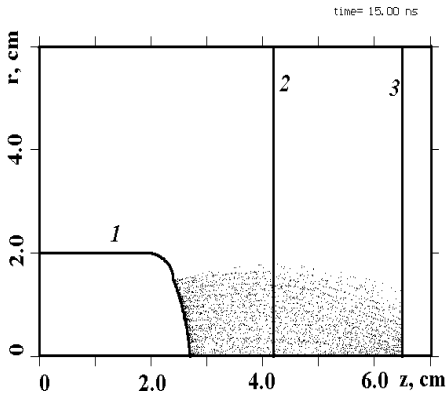

Fig. 1. The pattern of electron beam propagation calculated with KARAT code for l_1 = 15 mm and l_2 = 20 mm

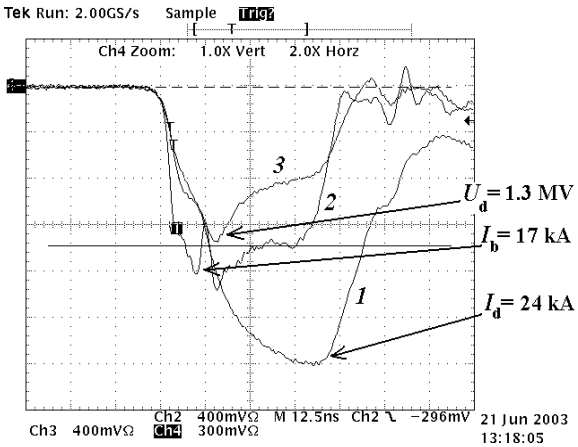

Fig. 2. Diode current (*1*), beam current (*2*), and diode voltage (*3*) for l_1 = 15 mm and l_2 = 23 mm.

The beam current density in its central part was found with a Faraday cup to be about 8 kA/cm^2. A diaphragm of 1.3 mm in diameter was placed in front of the Faraday cup during the measurement.

These investigations allowed us to form a homogeneous electron beam quite suitable for material science investigations, in particular for the case of studying the material spallation. Shown in Fig. 3 are the images from the front and rear surfaces of a copper specimen following a one-pass irradiation by an electron beam. On the front surface, a uniform 15 mm-diameter trace is seen, which resulted from material ablation. On the rear surface, there is a region of a virtually uniform spall of about 8 mm in diameter.

The measured pulse duration, electron energy, and electron beam density values were the input for simulating the temperature and stress fields in the specimen

under irradiation, whose simulation using a BETAIN1 code is described in the next section.

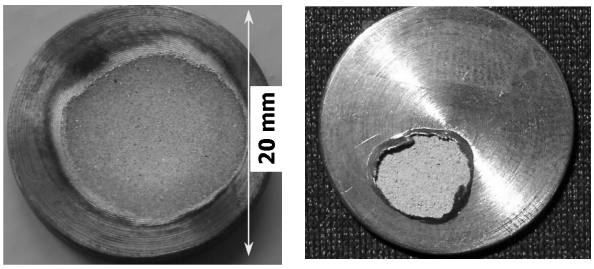

Fig. 3. Front (left) and rear (right) specimen surfaces upon a one-pass electron beam treatment

3. Numerical Investigations: BETAIN1 Code

An uncoupled set of equations of thermoelasticity can be applied to describe only the heat and strain processes in the irradiated target when the phase transformations are absent [16, 17]. The important advantage of the set of equations is the simplicity of numerical solution. However if a melting or moreover an intensive evaporation takes place in the irradiated target one should solve numerically a set of equations of condensed matter.

BETAIN1 numerical code based on solving hydrodynamic equations includes three conservation equations (mass, momentum, energy), the wide-range equation of state of material, and the kinetic equation for the electrons [18]. One-dimensional set of equations to be solved is writing in Lagrangian coordinates as follows:

the motion equation

$$\frac{dv_z}{dt} = \frac{1}{\rho}\frac{\partial \sigma_{zz}}{\partial z}, \qquad (1)$$

the continuity equation (mass conservation)

$$\frac{1}{V}\frac{dV}{dt} = \frac{\partial v_z}{\partial z}, \qquad (2)$$

the conservation equation of internal energy

$$\frac{dU}{dt} = \sigma_{zz}\frac{dV}{dt} + \frac{1}{\rho}\frac{\partial}{\partial z}\left(k\frac{\partial T}{\partial z}\right) + \frac{D(z,t)}{\rho}, \qquad (3)$$

where v_z is the velocity, ρ is the mass density, $V = 1/\rho$ is the specific volume, U is the internal energy of condensed matter, k is the heat conductivity, σ_{zz} is the component of stress tensor, which is writing as the sum of hydrostatic pressure (mean stress) and deviatoric stress as follows:

$$\sigma_{zz} = -P(\rho,T) + S_{zz}, \qquad (4)$$

herewith

$$\frac{dS_{zz}}{dt} = \frac{4}{3}\mu\frac{\partial v_z}{\partial z}; \quad \frac{dS_{xx}}{dt} = \frac{dS_{yy}}{dt} = \frac{2}{3}\mu\frac{\partial v_z}{\partial z}, \qquad (5)$$

$D(z,t)$ is the dose per unit time, describing energy delivery to the target

$$D(z,t) = \int d\Omega \int dT^{(b)} B(T^{(b)})\Psi(z,\Omega,T^{(b)}), \qquad (6)$$

where $T^{(b)}$ is the particle energy, $B(T^{(b)}$ is the specific energy loss, $\Psi(z,\Omega,T^{(b)})$ is the differential on angles and energies function describing a particles flow density and satisfying to the radiation tranfer equation

$$\hat{L}\Psi(z,\Omega,T^{(b)}) = S, \qquad (7)$$

where $\hat{L}$ is the transfer operator, and S is the source function of beam particles. The electron transfer model takes into consideration the elastic scattering processes, fluctuation energy losses in inelastic collisions, and secondary electron production.

The elastoplastic properties of a target material are described with the von Mises criteria

$$S_{xx}^2 + S_{yy}^2 + S_{zz}^2 \le \frac{2}{3}Y_0^2; \quad P_{\min} = -\frac{1}{3}Y_0, \qquad (8)$$

where Y_0 is the material yield strength.

The set of equation (1–8) is completed by the wide-range equation of state

$$P = P(\rho,T). \qquad (9)$$

The data calculated with the BETAIN1 numerical code include, in particular, the temperature, stresses, and mass density fields.

The in-depth distribution of mass density (curve *1*) and its gradient (curve *2*) in copper target of thickness 3 mm are shown in Fig. 4. The distribution is shown at the instant just before the stress wave reflection from the rear surface. The maximal value of density gradient is equal to 10^6 kg/m^4. Using the formula [5]

$$\dot{\varepsilon} = -\frac{C}{\rho}\frac{\partial \rho}{\partial z}, \qquad (10)$$

where C is the sound of velocity, one can determine the strain rate $\dot{\varepsilon}$, which is the important characteristic of a material loading, and in our case it was found to be about $5\cdot10^5$ s^{-1}.

Figure 5 presents the calculated stress wave behavior in a copper target at different instants of time. The electron beam parameters are the same as those given in Fig. 2. It is seen that irradiation by an electron beam forms a monopolar stress wave having an amplitude of 6 GPa near the surface. The wave propagates towards the rear surface of the target, with the amplitude initially decreasing quite fast and then more slowly and the full width increasing. For instance at a depth of 5 mm, the wave amplitude is 1.3 GPa while

its full width has increased from 0.65 to 1.34 mm. The average propagation rate of the stress wave is $4.8 \cdot 10^3$ m/s, which exceeds the sound velocity in copper; which allows one to refer to it as a shock wave.

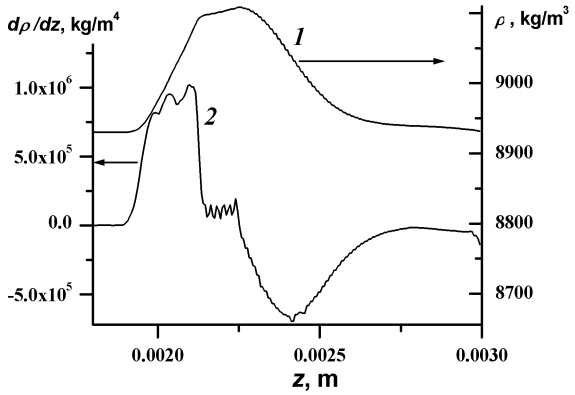

Fig. 4. The in-depth distribution of mass density (curve *1*) and its gradient (curve *2*) in copper target

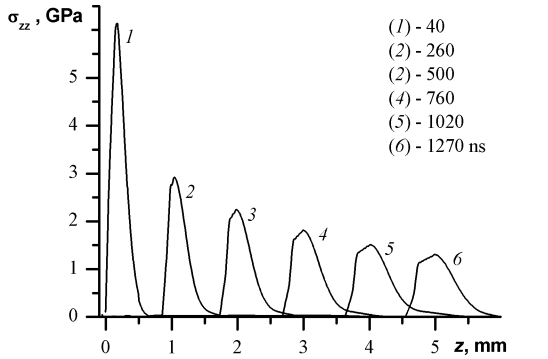

Fig. 5. Profiles of the stress wave in copper target at various points of time.

4. Spallation Experimental Results and Discussion

The spallation experiments were carried out with the gaps l_1 and l_2 equal to 15 and 23 mm, respectively. Copper specimens of diameter 20 mm and thickness from 2 to 6 mm were used. By measurements performed on a profilometer it has been established that the ablation region on the irradiated surface was 0.25–0.3 mm deep and up to 16 mm wide.

The specimens were cut normal to the irradiated surface; the sections were polished and examined in an optical microscope. Figure 6 shows the cross section of a copper specimen of thickness 2 mm after irradiation. It can be seen that a thin layer spalled off on the rear surface of the target. Although the spalled layer of the specimen is rather long, it remains unbroken. As the thickness of the target is increased, the spalled layer decreases in length (see Figs. 6 and 7). As can also be seen from these plots, the decrease in length of the spalled layer is accompanied by an increase in its depth. The depth of the spalled layer of a target as a function of the target thickness is given in Fig. 8. It can be seen that as the target thickness was increased from 2 to 5 mm, the depth of the spalled layer increased from 0.18 to 0.32 mm. The data fall satisfactorily on the dashed line, demonstrating a directly proportional relationship between these quantities. For the target of thickness 6 mm, no spallation was observed.

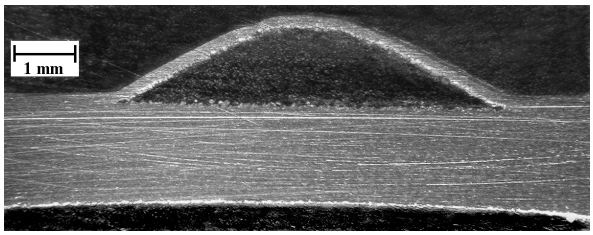

Fig. 6. The cross section of a copper specimen of thickness 2 mm after irradiation

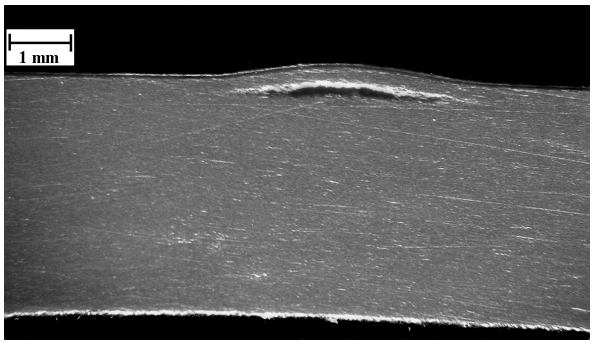

Fig. 7. The cross section of a copper specimen of thickness 4 mm after irradiation

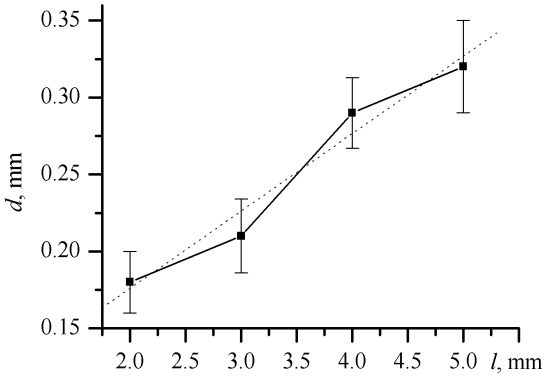

Fig. 8. The depth of the spalled layer (*d*) as a function of the thickness of the target (*l*)

The increase in depth of the spalled layer with the thickness of the target was also observed upon laser irradiation [5, 6]. This is accounted for by the fact that a shock wave in a thin target attenuates insignificantly and the stresses induced nearly behind the front of the wave upon its reflection are intense enough to cause spallation. For a thicker target, the attenuation of the wave is more substantial, and the stress intensity sufficient for spallation to take place is achieved not nearly behind the front, but closer to the wave peak, i.e., farther from the rear surface. Obviously, the same situation took place in our case where copper was irradiated with a relativistic high-current electron beam.

It should be noted that both the thickness of targets for which spallation is observed and the depth of the spalled layer for targets irradiated with a relativistic high-current electron beam are several times greater than the same parameters for laser-irradiated targets. This circumstance promotes materials science examinations of targets after irradiation.

Comparison of the experimental data on spallation with the calculations presented in Figs. 4 and 5 allows the conclusion that the spall strength of copper, which in fact corresponds to the amplitude of the stress wave at the rear surface of the thickest target for which spallation is still observed, is 1.1 GPa. This spall strength corresponds to the strain rate realized in our case that was equal to $5 \cdot 10^5$ s^{-1}. This result is in very good agreement with the summarized data on the spall strength of copper obtained with various methods of loading [7].

The morphology of spalled surface is substantially different from that of the ablation zone on the face surface. Scanning electron microscope of the surface upon spallation demonstrates that the fracture of copper is performed on the two scale levels (see Fig. 9).

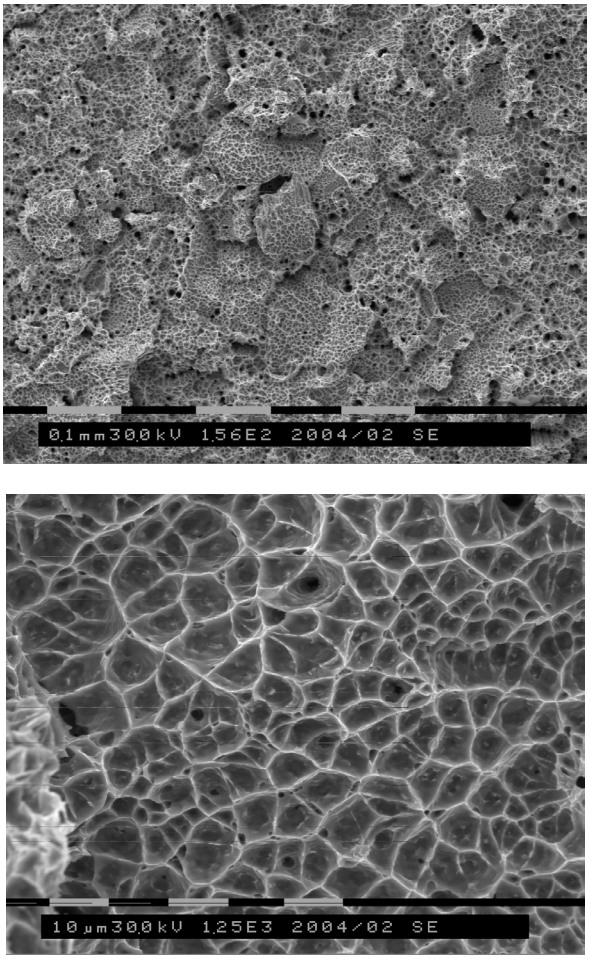

Fig. 9. SEM images of the surface upon spallation demonstrated both large-scale (upper image) and low-scale (lower image) level of fracture

The upper image on the Figure reveals the coarse-cell structure with a cell size of ~100 μm having the different shapes. The coarse cells are responsible for the large-scale level of the fracture. On the lower image it can be seen that these coarse cells have the fine-cell appearance with a fine-cell size of ~10 μm. The fine cells are responsible for the small-scale level of the fracture. The boundaries between the fine cells have dimensions of several tenths of a micrometer. This structure of the spallation surface is perhaps evidence of the dynamic mechanism of spallation, which is a sequence of processes of nucleation, growth, and coalescence of microvoids. It is possible that each fine cell is an observable region where microvoids have united in a colony; that is, such a region can be considered, by analogy with solidification of a melt, as a grain of a kind and the spallation process can be treated as a "condensed matter-void" phase transition.

5. Conclusions

1. Using the SINUS-7 accelerator, a pulsed relativistic electron beam suitable for materials science investigations has been obtained.

2. Optimum irradiation conditions have been found both for the realization of the rear spallation mode and for the treatment of a target in the mode of uniform face erosion.

3. It has been shown experimentally that as the target thickness is increased from 2 to 5 mm, the depth of the spalled layer increases from 0.18 to 0.32 mm, and these values are in an almost direct proportion to each other.

4. By comparison of experimental data and results of numerical simulations, it has been estimated that for the strain rate $5 \cdot 10^5$ s^{-1} that is realized in a target under the action of a relativistic high-current electron beam the spall strength of copper is 1.1 GPa.

Acknowledgments

The authors are grateful to I.M. Goncharenko and Yu.F. Ivanov for their help in preparation of specimens.

References

[1] G.E. Ozur, D.I. Proskurovsky, V.P. Rotshtein, and A.B. Markov, Laser and Particle Beams **21**, 157 (2003).

[2] G. Mueller, H. Bluhm, A. Heinzel, G. Schumacher, D. Strauss, A. Weisenburger, F. Zimmermann, V. Engelko, V. Shulov, N. Notchovnaia, *in: Proc. 6th Int. Conf. on Modification of Materials with Particle Beams and Plasma Flows*, Tomsk, Russia, 2002, pp. 328–331.

[3] D.I. Proskurovsky, V.P. Rotshtein, G.E. Ozur, A.B. Markov, D.S. Nazarov, V.A. Shulov, Yu.F. Ivanov, R.G. Buchheit, J. Vac. Sci and Technol. A **16 (4)**, 2480 (1997).

[4] G.I. Kanel, S.V. Razorenov, A.V. Utkin, V.E. Fortov, *Stress-wave phenomena in condensed matter*, Moscow, Yanus-K, 1996, 408 pp.
[5] S. Eliezer and I. Gilath, J. Appl. Phys. **67** (2), 715 (1990).
[6] M. Boustie and F. Cottet, J. Appl. Phys. **69** (11), 7533 (1991).
[7] V.E. Fortov, V.V. Kostin, and S. Elieser, J. Appl. Phys. **70** (8), 4524 (1991).
[8] H. Tamura, T. Kohama, K. Kondo, and M. Yoshida, J. Appl. Phys. **89** (6), 3520 (2001).
[9] E.K. Bonjushkin, B.L. Glushak, N.I. Zavada, S.A. Novikov, L.A. Platonova, N.I. Seljchenova, I.R. Trunin, A.Ya. Uchaev, N.A. Yukina, Prikladnaya mekhanika i tekhnicheskaya fizika (Rus) **37** (6), 105 (1996).
[10] A.I. Pavlovskii, E.K. Bonjushkin, A.Ya. Uchaev, S.A. Novikov, V.A. Tsukerman, N.I. Zavada, I.R. Trunin, Doklady acadimii nauk SSSR (Rus) **317** (6), 1376 (1991).
[11] A.M. Molitvin, Fizika i khimiya obrabotki materialov (Rus) **4**, 13 (2002).
[12] G.I. Kanel, S.V.Razorenov, V.E.Fortov, Doklady acadimii nauk SSSR (Rus) **275** (2), 369 (1984).
[13] I.P. Borin, S.A. Novikov, A.P. Pogorelov, V.A. Sinitsyn, ibid, **266** (6), 1377 (1982).
[14] S.D. Korovin, V.V. Rostov, Izvestiya vuzov. Fizika (Rus) **12**, 21 (1996).
[15] V.P. Tarakanov, *User Manual for Code KARAT*, Springfield, VA: BRA, 1992, 176 p.
[16] A.B. Markov, Yu.F. Ivanov, D.I. Proskurovsky, V.P.Rotshtein, *Materials and Manufacturing Processes* 14 (2), 205 (1999).
[17] G.A. Bleikher, V.P. Krivobokov, O.V. Pashenko, *Heat and mass transfer in solids induced by power beams of charged particles*, Novosibirsk, Nauka, 1999, 176 pp.
[18] A.P. Yalovets, A.E. Mayer, *in: Proc. 6th Int. Conf. on Modification of Materials with Particle Beams and Plasma Flows*, Tomsk, Russia, 2002, pp. 297–299.